Nanoscale

Accepted Manuscript

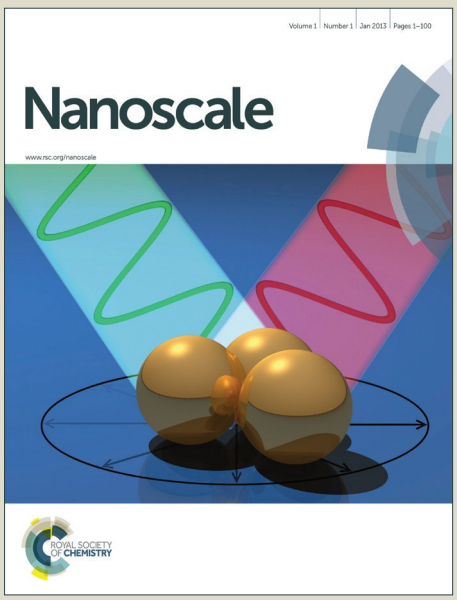

ROYAL SOCIETY OF CHEMISTRY

www.rsc.org/nanoscale

Nanoscale

ARTICLE

Size-controllable synthesis of Bi/Bi_2O_3 heterojunction nanoparticles using pulsed Nd:YAG laser deposition and metal-semiconductor-heterojunction-assisted photoluminescence

Received 00th January 20xx,
Accepted 00th January 20xx

DOI: 10.1039/x0xx00000x

www.rsc.org/

Ranjit A. Patil,[a] Mao-Kuo Wei,[b] P.-H. Yeh,[c] Jyun-Bo Liang,[a] Wan-Ting Gao,[a] Jin-Han Lin,[d] Yung Liou[d] and Yuan-Ron Ma*[a]

We synthesized Bi/Bi_2O_3 heterojunction nanoparticles at various substrate temperatures using the pulsed laser deposition (PLD) technique with a pulsed Nd:YAG laser. The Bi/Bi_2O_3 heterojunction nanoparticles consisted of Bi nanoparticles and Bi_2O_3 surface layers. The average diameter of the Bi nanoparticles and the thickness of the Bi_2O_3 surface layer are linearly proportional to the substrate temperature. The heterojunctions between the Bi nanoparticles and Bi_2O_3 surface layers, which are the metal-semiconductor heterojunctions, can strongly enhance the photoluminescence (PL) of the Bi/Bi_2O_3 nanoparticles, because the metallic Bi nanoparticles can provide massive free Fermi-level electrons for the electron transitions in the Bi_2O_3 surface layers. The enhancement of PL emission at room temperature by the metal-semiconductor-heterojunction make the Bi/Bi_2O_3 heterojunction nanoparticles potential candidates for use in optoelectronic nanodevices, such as light-emitting diodes (LEDs) and laser diodes (LDs).

Introduction

There are a variety of metal/metal-oxide heterojunction nanostructures that have attracted scientific attention because of their unique and significant properties.[1,2] Bi/Bi_2O_3 is one of the most popular of the metal/metal-oxide heterojunction nanostructures, and has been used in many applications, such as for hydrogen generation,[3] oxygen sensing,[4] photocatalysis,[5,6] superhydrophobicity,[7] and nanomechanics.[8] In addition to Bi_2O_3, the bismuth oxides have varying chemical forms, including Bi_2O_4,[9,10] Bi_4O_7,[9] and $Bi_2O_{2.33}$.[11] Obviously, Bi_2O_3 is the most stable bismuth oxide state, with six varying crystalline phases, including α-Bi_2O_3 (monoclinic phase), β-Bi_2O_3 (tetragonal phase), γ-Bi_2O_3 (bcc phase), δ-Bi_2O_3 (fcc phase), ε-Bi_2O_3 (orthorhombic phase) and w-Bi_2O_3 (triclinic phase). Among the six crystalline phases, α-Bi_2O_3 is much more frequently reported than β-Bi_2O_3. This is because monoclinic α-Bi_2O_3[12,13] and tetragonal β-Bi_2O_3[14,15] are the stable low-temperature and high-temperature forms, respectively, and that monoclinic α-Bi_2O_3 is easier to synthesize than tetragonal β-Bi_2O_3. Monoclinic α-Bi_2O_3 is a p-type semiconductor with a bandgap of ~2.8 eV,[16-18] while tetragonal β-Bi_2O_3 is an n-type semiconductor with a bandgap of ~2.5 eV.[18] Therefore, they can be designed for applications in heterojunctions[3-12] and opto-electronics.[13-18] Here, we discuss the metal-semiconductor-heterojunction-assisted photoluminescence (PL) emission mechanism for the Bi/Bi_2O_3 heterojunction nanoparticles. The Bi/Bi_2O_3 heterojunction nanoparticles comprise metallic Bi nanoparticles with Bi_2O_3 surface layers. The PL emissions that come from the Bi_2O_3 surface layers can be attributed to electron transitions from the conduction band, Fermi level (E_F), and donor state (E_D), respectively, to the valence bands in the Bi_2O_3 surface layers. These metallic Bi nanoparticles are helpful in the formation of PL emissions, because they provide plenty of free Fermi-level electrons to the Bi_2O_3 layers across the heterojunction. It is known that Bi is a semimetal, with its own unique Fermi surface.[19] Hence, the metallic Bi nanoparticles can enhance the PL emissions.

[a]Department of Physics, National Dong Hwa University, Hualien 97401, Taiwan
[b]Department of Materials Science and Engineering, National Dong Hwa University, Hualien 97401, Taiwan
[c]Department of Physics, Tamkang University, Tamsui, New Taipei City 25137, Taiwan
[d]Institute of Physics, Academia Sinica, Taipei 11529, Taiwan.

† Footnotes relating to the title and/or authors should appear here.
Electronic Supplementary Information (ESI) available: Diameter distribution of the Bi nanoparticles, and four band structures of metal-semiconductor heterojunctions. See DOI: 10.1039/x0xx00000x

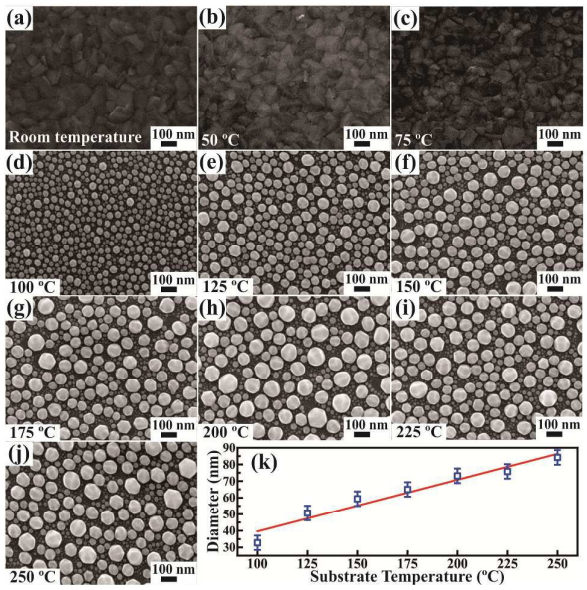

Fig. 1. FESEM images showing top views of the Bi thin films and nanoparticles on Si wafers at various substrate temperatures of (a) 25, (b) 50, (c) 75, (d) 100, (e) 125, (f) 150, (j) 175, (h) 200, (j) 225, and (j) 250 ºC, respectively. (k) Linear graph of the average diameter of the Bi nanoparticles *versus* substrate temperature.

In this study, Bi/Bi_2O_3 heterojunction nanoparticles were synthesized using the lower-energy pulsed laser deposition (PLD) technique with a pulsed Nd:YAG laser. Actually, there are two kinds of high- and low-energy PLD techniques. For example, PLD with an excimer laser of a few joules would be a high-energy system,[20-22] while a pulsed Nd:YAG laser of millijoules is a low-power system.[23,24] The high-energy PLD technique is used to synthesize high melting-point materials, including ceramics and oxides,[25-27] while the low-energy PLD method is exploited for the preparation of low melting-point materials, such as post-transition metals.[23,24,28-30] The synthesis of the Bi/Bi_2O_3 heterojunction nanoparticles included two processes. First, the Bi nanoparticles were grown on the Si substrates at various substrate temperatures of 100, 125, 150, 175, 200, 225, and 250 ºC, respectively. The average diameters of the Bi nanoparticles are linearly proportional to the substrate temperatures. Secondly, the surfaces of the Bi nanoparticles were oxidized in ambient air to produce Bi_2O_3 layers or shells, and then the Bi/Bi_2O_3 heterojunction nanoparticles were formed. The thicknesses of the Bi_2O_3 layers or shells also increased with the elevated substrate temperatures. As mentioned above, the Bi/Bi_2O_3 heterojunction nanoparticles were found to enhance the PL emissions. As the incident laser supplies thermal energy to the free electrons of the metallic Bi nanoparticles, they easily overcome the Ohmic barrier and move to the Bi_2O_3 layers. This is because the as-synthesized Bi_2O_3 layers are *n*-type semiconductors, so that Ohmic contacts, which are one of the metal-semiconductor heterojunctions, are formed at the interfaces between the Bi nanoparticles and Bi_2O_3 layers. The metallic Bi nanoparticles can provide the majority free electrons for the electron-hole recombination that gives rise to strong PL emissions. These Bi/Bi_2O_3 heterojunction nanoparticles are potential candidates for use in optoelectronic nanodevices, such as light-emitting diodes (LEDs) and laser diodes (LDs), because they have good and effective visible-light emissions at room temperature.

Experimental

Synthesis of Bi/Bi_2O_3 heterojunction nanoparticles

The Bi/Bi_2O_3 heterojunction nanoparticles were synthesized on Si substrates in a high-vacuum PLD system (AdNaNo-Tek, PLD-12L) with a Q-switched and pulsed Nd:YAG laser (LOTIS TII, LS-2134UTF). Tablets of Bi (99.99 % pure, ~9 mm wide and ~ 3 mm high) were placed on a rotating holder as target materials in the PLD chamber. The distance between the target and Si substrate was 50 mm. Once the pressure was pumped down to $\sim 1\times10^{-7}$ torr, a pulsed laser (266 nm), which possessed an energy of 50 mJ and a pulse duration of 6 ns, was utilized to perform laser ablation for 45 min. The pulsed laser beam of ~1.77 mJ/mm^2 was focused on the Bi-tablet targets by a lens incident at an angle of 60° to the target surface. Temperature plays a very significant role in the growth of nanostructures,[31-35] so to observe this the substrates were kept at various temperatures during the deposition process. Various Bi thin films and nanoparticles on Si wafers were prepared at the various substrate temperatures of 25, 50, 75, 100, 125, 150, 175, 200, 225, and 250 ºC, respectively. The surfaces were oxidized in ambient air to produce Bi_2O_3 layers or shells, and then the Bi/Bi_2O_3 heterojunction nanoparticles were formed. The thicknesses of the Bi_2O_3 layers or shells increased with the elevated substrate temperatures.

Characterization of Bi/Bi_2O_3 heterojunction nanoparticles

The surface morphology and elemental information of the as-synthesized Bi/Bi_2O_3 heterojunction nanoparticles were examined using a field-emission scanning electron microscope (FESEM, JEOL JSM-6500F) equipped with an energy dispersive spectrometer (EDS, Oxford instrument INCA, X-sight 7557). The crystalline structures of the Bi/Bi_2O_3 heterojunction nanoparticles were verified by an X-ray diffractometer (XRD, Philips, X'Pert Pro) with Cu Kα radiation (1.541 Å) and a transmission electron microscope (TEM, JOEL JEM-2100) with a selected-area electron diffractometer (SAED). The chemical compositions of the Bi/Bi_2O_3 heterojunction nanoparticles were quantitatively analyzed based upon an X-ray photoelectron spectrometer (XPS, Thermo Scientific, K-Alpha) with an Al Ka beam of 1486.6 eV and an ion gun. The PL properties of the Bi/Bi_2O_3 heterojunction nanoparticles were verified using a spectrometer (Ocean Optics, QE65000) equipped with a charge-coupled device (CCD) detector array and a pumping light source from a 325 nm He-Cd laser.

Results and discussion

The FESEM images in Figs. 1(a)-1(j) show top views of Bi thin films and nanoparticles on Si wafers with the various substrate temperatures of 25, 50, 75, 100, 125, 150, 175, 200, 225, and 250 ºC, respectively. The surface morphologies that appear in Figs. 1(a)-1(c) look rough, but many Bi nanoparticles are observed in Figs.

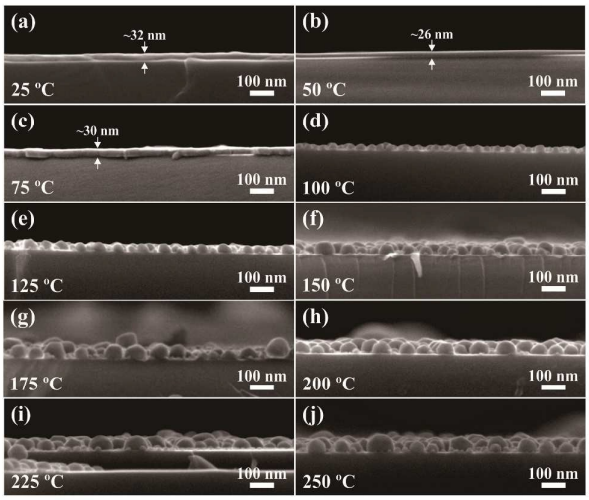

Fig. 2. FESEM images showing side views (90º to the surface normal direction) of the Bi thin films and nanoparticles on Si wafers at various substrate temperatures of (a) 25, (b) 50, (c) 75, (d) 100, (e) 125, (f) 150, (j) 175, (h) 200, (j) 225, and (j) 250 ºC, respectively.

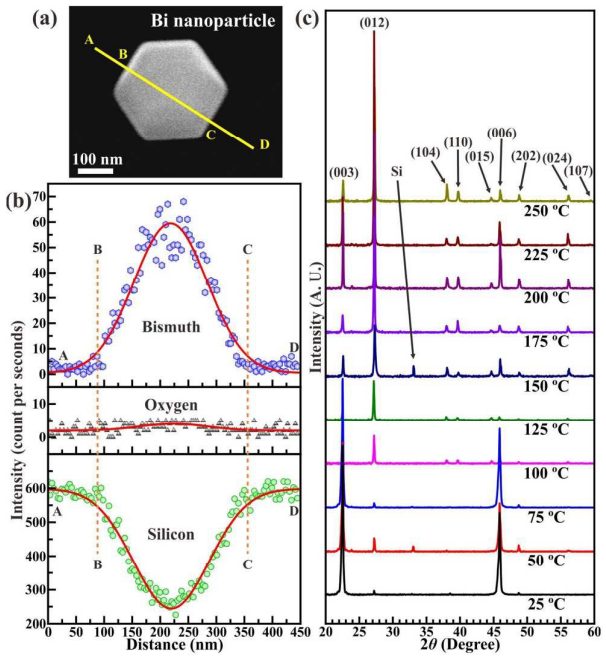

Fig. 3. (a) FESEM image showing a single Bi hexagonal nanoparticle synthesized at a substrate temperature of 250 ºC. The EDS intensities of Bi, O and Si can be detected along the yellow line that runs across this image from A to D and passes through the Bi nanoparticle from B to C. (b) EDS intensity-profiles of Bi, O and Si as functions of distance along segment AD. (c) Ten XRD spectra for the Bi thin film and nanoparticles synthesized at substrate temperatures of 25, 50, 75, 100, 125, 150, 175, 200, 225, and 250 ºC, respectively. All ten XRD spectra are similar in patterns, indicating that the as-synthesized Bi thin film and nanoparticles formed at various substrate temperatures consist of the same crystalline phases.

1(d)-1(j). Some of the Bi nanoparticles have facets, indicating they possess a crystalline structure. There is a linear increase in the average diameter of the Bi nanoparticles with the elevation of the substrate temperature. The linear graph in Fig. 1(k) shows the average diameter of the Bi nanoparticles *versus* substrate temperature. A lognormal distribution function[33] is used to acquire the average diameter and the fit of the diameter distributions of the Bi nanoparticles. The statistical histograms (see Fig. S1, Supplementary Information) display the diameter distributions of the Bi nanoparticles synthesized at substrate temperatures of 100, 125, 150, 175, 200, 225, and 250 ºC, respectively. All the fitting parameters such as the majority distribution, average diameter, and standard deviation are shown in Table S1 (Supplementary Information).

The FESEM images in Fig. 2 show side views (90º to the surface normal direction) of the as-synthesized Bi thin films and nanoparticles illustrated in Figs. 1(a)-1(j), respectively. Figs. 2(a)-2(c) display Bi nanoscale thin films of ~32, ~26 and ~30 nm grown on Si wafers at substrate temperatures of 25, 50, and 75 ºC, respectively, while Figs. 2(d)-2(j) illustrate Bi nanoparticles that formed on Si wafers at substrate temperatures of 100, 125, 150, 175, 200, 225 and 250 ºC. It can be seen that the thin films preferentially grow at low substrate-temperatures (<100 ºC), while the high temperatures (≥100 ºC) are favorable for the formation of Bi nanoparticles. Hence, there are two kinds of growth modes, the Frank-van-der-Merwe (layer-by-layer)[36] and Wolmer-Weber (island)[36] growth modes. During evaporation of the Bi tablets onto the Si wafer by the PLD technique, the initial kinetic energy carried by the Bi atoms is diffuse onto the Si substrates. The heating of the substrate obviously provides thermal energy, which enhances the surface diffusion of the Bi atoms. However, when the substrate temperature is not high enough, the total energy (≡kinetic energy *plus* thermal energy) supports a diffusive force that cannot overcome the interaction between the atoms and the substrate surface. In other words, the interactions between the diffusing atoms are smaller than those between the atoms and the substrate surfaces, and then thin films are preferentially formed. On the other hand, when the substrate temperature is high enough, the diffusive force supported by the total energy becomes superior to the interaction between atoms and substrate surfaces. The interactions between the diffusing atoms are thus larger than those between the atoms and the substrate surfaces, so that nanoparticles (or nano-islands) are formed. As seen from these results, we can easily control the growth of thin films or nanoparticles of Bi using only the substrate temperature.

EDS is a high spatial-resolution tool utilized for qualitative analysis of the chemical composition on the surface, from which we can identify the elemental distribution on the nanoscale and specify whether the Bi nanoparticles become oxidized in the high vacuum chamber to form bismuth oxides. The FESEM image in Fig. 3(a) shows a single Bi hexagonal nanoparticle of ~280 nm wide synthesized at a substrate temperature of 250 ºC. The EDS intensities of Bi, O and Si can be detected along the yellow line that runs across this image from A to D and passes through the Bi nanoparticle from B to C. Fig. 3(b) illustrates the EDS intensity-profiles of Bi, O and Si as functions of distance along the segment AD. The Bi intensity is rich, but the O intensity is almost zero. The Si intensity comes from the Si substrate, but decreases due to the presence of the Bi nanoparticles. The absence of O intensity implies

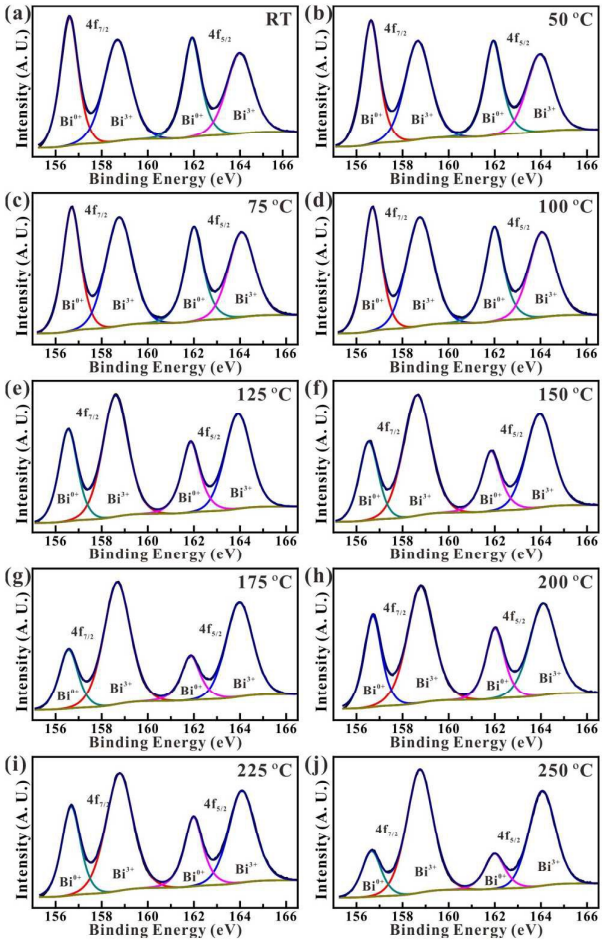

Fig. 4. Ten XPS spectra for Bi thin films and nanoparticles synthesized at substrate temperatures of (a) 25, (b) 50, (c) 75, (d) 100, (e) 125, (f) 150, (g) 175, (h) 200, (i) 225, and (j) 250 ºC, respectively. All the XPS spectra have the same Bi^{0+} $4f_{7/2}$, Bi^{0+} $4f_{5/2}$, Bi^{3+} $4f_{7/2}$, and Bi^{3+} $4f_{5/2}$ peaks, but the peaks have various intensities ($I^{0+}{}_{7/2}$, $I^{0+}{}_{5/2}$, $I^{3+}{}_{7/2}$, $I^{3+}{}_{5/2}$).

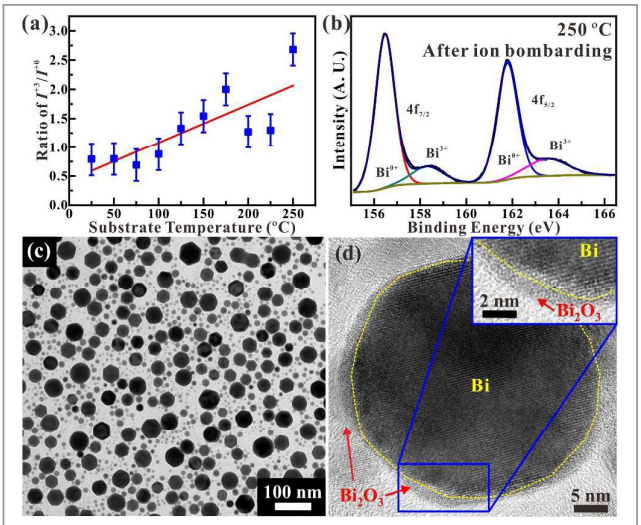

Fig. 5. (a) Linear graph of the intensity ratio ($=I^{3+}/I^{0+}=(I^{3+}{}_{7/2}+I^{3+}{}_{5/2})/(I^{0+}{}_{7/2}+I^{0+}{}_{5/2})$) of the total B^{3+} 4f to B^{0+} 4f peaks (in Fig. 4) *versus* substrate temperature. The fitting result shows that the intensity ratio linearly increased with the elevation of the substrate temperature. (b) XPS spectra of the Bi/Bi_2O_3 heterojunction nanoparticles (synthesized at the substrate temperature of 250 ºC) after ion milling. The TEM image showing (c) a group of the Bi/Bi_2O_3 heterojunction nanoparticles and (d) a single Bi/Bi_2O_3 heterojunction nanoparticle, synthesized at a substrate temperature of 250 ºC. The portion enclosed by yellow dashed-circle is Bi, but that outside the yellow dashed-circle is Bi_2O_3. The high-resolution TEM image in the inset clearly shows the Bi/Bi_2O_3 heterojunction or interface between the Bi core and Bi_2O_3 surface layer.

that the Bi nanoparticle is still pure Bi, including no bismuth oxides at all. Hence, the Bi nanoparticles may not be able to be oxidized into bismuth oxides in the high vacuum chamber. The XRD patterns can be called the fingerprints of crystalline materials, revealing details of their crystalline structure and crystal growth formation during synthesis. Fig. 3(c) shows the ten XRD spectra for the Bi thin films and nanoparticles synthesized at substrate temperatures of 25, 50, 75, 100, 125, 150, 175, 200, 225, and 250 ºC, respectively. All ten XRD spectra have the same patterns, indicating that the as-synthesized Bi thin film and nanoparticles consist of the same crystalline phases regardless of the various substrate temperatures. The diffraction peaks at 2ϑ= 22.6º, 27.2º, 38.1º, 39.7º, 44.7º, 46.1º, 48.8º, 56.2º, and 59.6º correspond respectively to the (003), (012), (104), (110), (015), (006), (202), (024), and (107) planes of the rhomb-centered hexagonal Bi phase in the space group, with lattice constants of a=b=0.4535 nm, c=1.1814 nm, α=β=90º, and γ=120º (ICSD 64704). Therefore, the XRD results cannot offer any evidence that the Bi thin film and nanoparticles are oxidized. In addition, although the Bi thin films and nanoparticles have the same crystalline structures, there are strong diffraction intensities located at different diffraction angles (2ϑ). For example, while the Bi thin films possess strong diffraction intensities at the (003) and (006) planes, the Bi nanoparticles have the strong diffraction intensities at the (003), (012) planes. It can be seen from this that the crystalline orientations of the Bi thin films are different from those of the Bi nanoparticles.

It is known that EDS and XRD are good techniques for providing information from deep inside Bi thin films and nanoparticles, while the XPS technique can give information from the surface, ~10 nm deep. Fig. 4 shows a series of XPS spectra for the Bi thin films and nanoparticles synthesized at substrate temperatures of 25, 50, 75, 100, 125, 150, 175, 200, 225, and 250 ºC, respectively. All the XPS spectra show the same Bi^{0+} $4f_{7/2}$, Bi^{0+} $4f_{5/2}$, Bi^{3+} $4f_{7/2}$, and Bi^{3+} $4f_{5/2}$ peaks, but the peaks have various intensities ($I^{0+}{}_{7/2}$, $I^{0+}{}_{5/2}$, $I^{3+}{}_{7/2}$, $I^{3+}{}_{5/2}$). The Bi^{3+} $4f_{7/2}$ and Bi^{3+} $4f_{5/2}$ peaks indicate that all the surfaces of the Bi thin films and nanoparticles are oxidized to become Bi_2O_3 layers in the ambient air. This indicates that the Bi thin films and nanoparticles are easily oxidized to become Bi/Bi_2O_3 heterojunction thin films and nanoparticles. In Figs. 4(a)-4(d), the intensities ($I^{0+}{}_{7/2}$, $I^{0+}{}_{5/2}$) of the Bi^{0+} $4f_{7/2}$ and Bi^{0+} $4f_{5/2}$ peaks are higher than those ($I^{3+}{}_{7/2}$, $I^{3+}{}_{5/2}$) of the Bi^{3+} $4f_{7/2}$ and Bi^{3+} $4f_{5/2}$ peaks, while in Figs. 4(e)-4(j), the intensities ($I^{0+}{}_{7/2}$, $I^{0+}{}_{5/2}$) of the Bi^{0+} $4f_{7/2}$ and Bi^{0+} $4f_{5/2}$ peaks are lower than those ($I^{3+}{}_{7/2}$, $I^{3+}{}_{5/2}$) of the Bi^{3+} $4f_{7/2}$ peaks. These intensity results suggest that the higher substrate temperatures not only make the diameters of the Bi nanoparticles larger, but also allow the Bi_2O_3 layers to be thicker.

The linear graph in Fig. 5(a) displays the intensity ratio ($\equiv I^{3+}/I^{0+}=(I^{3+}_{7/2}+I^{3+}_{5/2})/(I^{0+}_{7/2}+I^{0+}_{5/2})$) *versus* substrate temperature of the total B^{3+} 4f to B^{0+} 4f peaks (in Fig. 4). The data in Fig. 5(a) show an obvious linear fit, indicating that the higher the substrate temperature, the larger the intensity ratio, and the more oxidized the surfaces of the Bi thin films and nanoparticles. Thus, there also may be a linear increase in the thicknesses of the Bi_2O_3 layers with the elevation of the substrate temperatures. To verify the formation of the Bi_2O_3 layer on the surfaces of the Bi thin film and Bi nanoparticles, an ion gun was used to remove the surface of Bi nanoparticles synthesized at a substrate temperature of 250 ºC. Fig. 5(b) shows the XPS spectra of the Bi/Bi_2O_3 heterojunction nanoparticles (synthesized at the substrate temperature of 250 ºC) after ion milling. It is obvious that the intensities ($I^{0+}_{7/2}$, $I^{0+}_{5/2}$) of the Bi^{0+} $4f_{7/2}$ and Bi^{0+} $4f_{5/2}$ peaks are much larger than those ($I^{3+}_{7/2}$, $I^{3+}_{5/2}$) of the Bi^{3+} $4f_{7/2}$ and Bi^{3+} $4f_{5/2}$ peaks, confirming that the Bi nanoparticles have Bi_2O_3 layers on the surfaces. TEM is a powerful technique for examining the fine crystalline structures. The TEM image in Fig. 5(c) displays a group of Bi/Bi_2O_3 heterojunction nanoparticles synthesized at a substrate temperature of 250 ºC. The high-resolution TEM image in Fig. 5(d) illustrates a single Bi/Bi_2O_3 heterojunction nanoparticle from Fig. 5(c). The very thin Bi_2O_3 layer (<3nm) on the surface of the single Bi nanoparticle can be clearly seen, but the surface Bi_2O_3 layer looks amorphous, not crystalline. The TEM results confirm that the surfaces of the Bi thin film and nanoparticles are easily oxidized in ambient air, and the surface Bi_2O_3 layers have an amorphous structure.

PL spectroscopy is an excellent optical technique for examining the electron transitions and electronic information in the search for impurities, defects, and bandgaps in semiconductor materials. Fig. 6(a) shows the room-temperature PL spectra of Bi/Bi_2O_3 heterojunction nanoparticles synthesized at a substrate temperature of 175 ºC. Actually, the PL spectra of the Si substrate and Bi/Bi_2O_3 heterojunction nanoparticles synthesized at substrate temperatures of 100, 150, and 250 ºC (see Fig. S2 , Supplementary Information) are also taken. The PL emissions are observed over a wide wavelength range from 300 to 950 nm, and the PL spectra can be decomposed into three emission peaks centered at 492.9, 588.1, and 716.1 nm, corresponding to the energies of ~2.5, ~2.1, and ~1.7 eV, respectively. The inset to Fig. 6(a) shows a schematic diagram of the green-, red- and infrared-light emitted from the Bi/Bi_2O_3 heterojunction nanoparticles that comprise the inner metallic Bi nanoparticles and Bi_2O_3 layers. The color space chromaticity diagram in Fig. 6(b) shows the colors of the PL emissions from the Bi/Bi_2O_3 heterojunction nanoparticles. The Bi/Bi_2O_3 heterojunction nanoparticles obviously appear to be cyan, although the color actually consists of three main light emissions of green-, red- and infrared-light. The schematic diagram in Fig. 6(c) shows the electron transitions and PL emissions in the metal-semiconductor heterojunction for a metallic Bi nanoparticle in contact with the Bi_2O_3 layer, namely the Bi/Bi_2O_3 heterojunction nanoparticle. It is known that there are four kinds of metal semiconductor contacts, including two Schottky and two Ohmic contacts (see Fig. S3, Supplementary Information) for n-type and p-type semiconductors. Since the work function (4.22 eV) of Bi is smaller than that (6.23 eV) of Bi_2O_3,[3] the heterojunction of Bi/Bi_2O_3 is an Ohmic contact. Also, the observed PL emissions indicate the Bi_2O_3 layers to be *n*-type

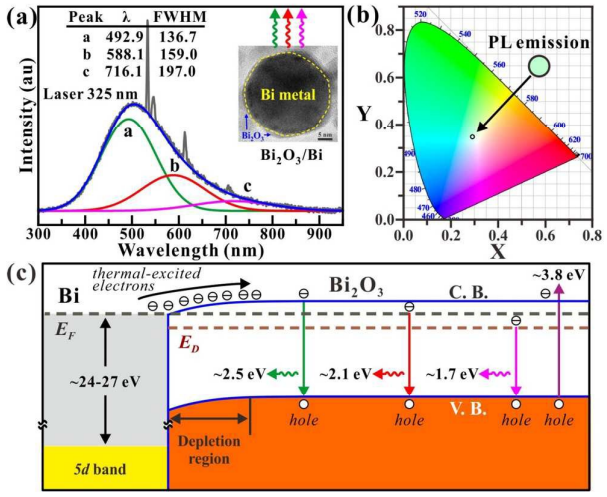

Fig. 6. (a) Room-temperature PL spectra of the Bi/Bi_2O_3 heterojunction nanoparticles synthesized at a substrate temperature of 175 ºC. The inset shows a schematic diagram of the green-, red- and infrared-light emitted from the Bi/Bi_2O_3 heterojunction nanoparticles that comprise the inner metallic Bi nanoparticles and Bi_2O_3 layers. (b) Color space chromaticity diagram showing the cyan color of the PL emissions from the Bi/Bi_2O_3 heterojunction nanoparticles. (c) Schematic diagram of the band structure for the electron transitions and PL emissions in the Bi/Bi_2O_3 heterojunction nanoparticles with the Ohmic metal-semiconductor heterojunctions.

semiconductors, because *p*-type Bi_2O_3 cannot support the PL emissions of ~2.1, and ~1.7 eV, which represent the electron transitions from the Fermi level (E_F) and the donor state (E_D) to the valence band. Of course, the PL emissions of ~2.5 eV embody the electron transitions between the conduction band and the valence band, which are called the near band edge (NBE) transitions.[17]

When the incident 325-nm laser (indicated by the upward pointing purple arrow) excites electrons from the valence band to the conduction band, holes are created in the valence band. The majority electrons lying in the conduction band and the Fermi level immediately drop down to recombine with the holes created in the valence band, and then the green light (indicated by the downward pointing green arrow) of 492.9 nm and the red light (indicated by the downward pointing red arrow) of 588.1 nm are emitted. In fact, the metallic Bi nanoparticles not only inject plenty of free electrons to the E_F, but also massive free electrons to the conduction bands. This is because the heat from the incident laser gives the massive free electrons thermal energy to overcome the small Ohmic contact barrier, so the thermal-excited electrons in the metallic Bi nanoparticles can move to the conduction band in the Bi_2O_3 layer. The PL intensity of 492.9 nm is higher than that of 588.1 nm, indicating more electrons are injected to the conduction band than the E_F. In addition, when the minority electrons lying in the E_D fall to the valence band, the recombination of the electrons and holes can give the infrared light (indicated by the downward pointing pink arrow) of 716.1 nm. Note that the observed PL emissions cannot come from the metallic Bi nanoparticles, because the 5*d* electronic band is ~24-27 eV, far from the E_F of the metallic Bi nanoparticles. Therefore, in this study, it is found that the metal-semiconductor-heterojunctions can enhance PL emissions of the *n*-type metal-

oxides or semiconductors, giving them the potential for use in optoelectronic nanodevices, such as light-emitting diodes and laser diodes.

Conclusions

In this study, Bi/Bi_2O_3 heterojunction nanoparticles were synthesized at various substrate temperatures using the pulsed laser deposition (PLD) technique with a pulsed Nd:YAG laser. The Bi/Bi_2O_3 heterojunction nanoparticles were comprised of Bi nanoparticles and *n*-type Bi_2O_3 surface layers. The average diameter of the Bi nanoparticles and the thickness of the Bi_2O_3 surface layer were strongly dependent on the substrate temperature, and linearly proportional to the substrate temperature. The Bi/Bi_2O_3 heterojunction nanoparticles were found to enhance the PL emissions, because the metallic Bi nanoparticles provided massive free Fermi-level electrons to the Bi_2O_3 surface layers. Since the Bi_2O_3 surface layers are *n*-type semiconductors and the work function is larger than that of the metallic Bi nanoparticles, Ohmic contacts form at the interfaces between the Bi nanoparticles and Bi_2O_3 layers. Heat from a laser is incident to the Bi/Bi_2O_3 heterojunction nanoparticles supplies thermal energy to the free electrons of the metallic Bi nanoparticles. The massive thermal-excited free electrons can easily overcome the Ohmic barrier and move to the conduction band in the Bi_2O_3 layers facilitating electron-hole recombination from the conduction band and the E_F to the valence band. Therefore, the enhancement of PL emission at room temperature by the metal-semiconductor-heterojunction make the Bi/Bi_2O_3 heterojunction nanoparticles potential candidates for use in optoelectronic nanodevices, such as light-emitting diodes (LEDs) and laser diodes (LDs).

Acknowledgements

The authors would like to thank the Ministry of Science and Technology, Taiwan for their financial support of this research under Contract Nos. MOST-103-2112-M-259-006-MY2, MOST-102-2923-M-259-001-MY3, and MOST 103-2811-M-259-014.

Notes and references

1 A. M. Smith and S. Nie, *Acc. Chem. Res.* 2010, **43**, 190-200.
2 R. S. Devan, R. A. Patil, J.-H. Lin and Y.-R. Ma, *Adv. Funct. Mater.* 2012, **22**, 3326-3370.
3 C. Li, J. Zhang and K. Liu, *Int. J. Electrochem. Sci.* 2012, **7**, 5028-5034.
4 J. Lim, A. Marien, K. Rosseel, A. Aerts and J. Van den Bosch, *J. Nucl. Mater.* 2012, **429**, 270-275.
5 L. Qu, Z. Luo and C. Tang, *Mater. Res. Bull.* 2013, **48**, 4601-4605.
6 S. Chu, C. Yang, C. Niu, Z. Li, J. Wang, X. Su, *Mater. Lett.* 2014, **136**, 366-370.
7 L. Cao, X. Lu, F. Pu, X. Yin, Y. Xia, W. Huang and Z. Li, *Appl. Surf. Sci.* 2014, **288**, 558-563.
8 R. Domingo-Roca, D. Esque-de los Ojos, M. Guerrero, E. Pellicer, M.D. Baro, S. Surinach and J. Sort, *Mater. Sci. Eng. A* 2015, **626**, 150-158.
9 A. S. Prakash, C. Shivakumara, M. S. Hegde, L. Dupont and J. M. Tarascon, *Mater. Res. Bull.* 2007, **42**, 707-712.
10 A. Hameed, T. Montini, V. Gombac and P. Fornasiero, *J. Am. Chem. Soc.* 2008, **130**, 9658-9659.
11 G. L. Fang, G. Chen, J. Q. Liu and X. Wang, *J. Phys. Chem. C* 2010, **114**, 864-867.
12 J. Hou, C. Yang, Z. Wang, W. Zhou, S. Jiao and H. Zhu, Appl. Catal. B-Environ. 2013, **142-143**, 504-511.
13 L. Zhang, W. Wang, J. Yang, Z. Chen, W. Zhang, L. Zhou and S. Liu, *Appl. Catal. A-General.* 2006, **308**, 105-110.
14 L. Kumari, J.-H. Lin and Y.-R. Ma, *J. Phys.: Condens. Matter.* 2007, **19**, 406204.
15 L. Kumari, J.-H. Lin and Y.-R. Ma, *Nanotechnology* 2007, **18**, 29560.
16 M. Ge, C. Cao, S. Li, S. Zhang, S. Deng, J. Huang, Q. Li, K. Zhang, S. S. Al-Deyab and Y. Lai, *Nanoscale* 2015, **7**, 11552-11560.
17 K. C. Chitrada, K. S. Raja, R. Gakhar and D. Chidambaram, *J. Electrochem. Soc.* 2015, **162**, H380-H391.
18 L. Shan, G. Wang, D. Li, X. San, L. Liu, L. Dong and Z. Wu, *Dalton Trans*. 2015, **44**, 7835-7843.
19 F. Y. Yang, K. Liu, K. Hong, D. H. Reich, P. C. Searson and C. L. Chien, *Science* 1999, **284**, 1335-1337.
20 P. R. Willmott and J. R. Huber, *Rev. Mod. Phys.* 2000, **72**, 315-328
21 E.-M. Choi, S.-G. Jung, N. H. Lee, Y.-S. Kwon, W. N. Kang, D. H. Kim, M.-H. Jung, S.-I. Lee and L. Sun, *Appl. Phys. Lett.* 2009, **95**, 062507.
22 V. Kekkonen,·A. Hakola,·J. Likonen,·Y. Ge and·T. Kajava, *Appl Phys A* 2012, **108**, 423-430.
23 H. Cui, P. Liu and G. W. Yang, *Appl. Phys. Lett.* 2006, **89**, 153124.
24 W.-O. Siew,·W.-K. Lee,·H.-Y. Wong,·T.-K. Yong,·S.-S. Yap and·T.-Y. Tou, *Appl. Phys A* 2010, **101**, 627-632.
25 T. Fix, C. Ulhaq-Bouillet, S. Colis, and A. Dinia, G. Bertoni, J. Verbeeck, and G. Van Tendeloo, *Appl. Phys. Lett.* 2007, **91**, 023106.
26 Y. Sun, R. P. Doherty, J. L. Warren and M. N. R. Ashfold, *Chem. Phys. Lett.* 2007, **447**, 257-262.
27 Y. Ichino, Y. Yoshida, T. Yoshimura, Y. Takai, M. Yoshizumi, T. Izumi and Y. Shiohara, *Phys. C* 2010, **470**, S1003-S1004.
28 M. A. Pushkin, V. V. Lebid'ko, V. D. Borman, V. N. Tronin, V. I. Troyan and I. Smurov, *Appl. Surf. Sci.* 2006, **252**, 4425-4428.
29 N. Pryds, J. Schou and S. Linderoth, *Appl. Surf. Sci.* 2007, **253**, 8231-8234.
30 A. T. T. Koh, Y. M. Foong and D. H.C. Chua, *Diam. Relat. Mater.* 2012, **25**, 98-102.
31 J.-H. Lin, R. A. Patil, M.-A. Wu, L.-G. Yu, K.-D. Liu, W.-T. Gao, R. S. Devan, C.-H. Ho, Y. Liou and Y.-R. Ma, *J. Mater. Chem. C* 2014, **2**, 8667-8672.
32 R. A. Patil, R. S. Devan, J.-H. Lin, Y.-R. Ma, P. S. Patil and Y. Liou, *Sol. Energy Mater. Sol. Cells* 2013, **112**, 91-96.
33 R. A. Patil, R. S. Devan, J.-H. Lin, Y. Liou and Y.-R. Ma, *Sci. Rep.* 2013, **3**, 3070.
34 R. S. Devan, C.-L. Lin, J.-H. Lin, T.-K. Wen, R. A. Patil and Y.-R. Ma, *J. Nanosci. Nanotechnol.* 2013, **13**, 1001-1005.
35 J.-H. Lin, Y.-J. Huang, Y.-P. Su, C.-A. Liu, R. S. Devan, C.-H. Ho, Y.-

P. Wang, H.-W. Lee, C.-M. Chang, Y. Liou and Y.-R. Ma, *RSC Adv.* 2012, **2**, 2123-2127.

36 E. Bauer, *Z. Kristall.* 1958, **110**, 372-394.